TISSUE ENGINEERING: Part A
Volume 27, Numbers 23 and 24, 2021

DOI: 10.1089/ten.tea.2020.0347

termis
Tissue Engineering
& Regenerative Medicine
International Society

ORIGINAL ARTICLE

Investigation of a Prevascularized Bone Graft for Large Defects in the Ovine Tibia

Yunzhi Peter Yang, PhD,[1–3] Benjamin C. Gadomski, PhD,[4] Arnaud Bruyas, PhD,[1] Jeremiah Easley, DVM,[5] Kevin M. Labus, PhD,[4] Brad Nelson, DVM,[5] Ross H. Palmer, DVM,[5] Holly Stewart, DVM,[5] Kirk McGilvray, PhD,[4] Christian M. Puttlitz, PhD,[4] Dan Regan, PhD, DVM,[6] Alexander Stahl, PhD,[1,7] Elaine Lui, BS,[1,8] Jiannan Li, PhD,[1] Seyedsina Moeinzadeh, PhD,[1] Sungwoo Kim, PhD,[1] William Maloney, MD,[1] and Michael J. Gardner, MD[1]

In vivo bioreactors are a promising approach for engineering vascularized autologous bone grafts to repair large bone defects. In this pilot parametric study, we first developed a three-dimensional (3D) printed scaffold uniquely designed to accommodate inclusion of a vascular bundle and facilitate growth factor delivery for accelerated vascular invasion and ectopic bone formation. Second, we established a new sheep deep circumflex iliac artery (DCIA) model as an *in vivo* bioreactor for engineering a vascularized bone graft and evaluated the effect of implantation duration on ectopic bone formation. Third, after 8 weeks of implantation around the DCIA, we transplanted the prevascularized bone graft to a 5 cm segmental bone defect in the sheep tibia, using the custom 3D printed bone morphogenic protein 2 (BMP-2) loaded scaffold without prior *in vivo* bioreactor maturation as a control. Analysis by micro-computed tomography and histomorphometry found ectopic bone formation in BMP-2 loaded scaffolds implanted for 8 and 12 weeks in the iliac pouch, with greater bone formation occurring after 12 weeks. Grafts transplanted to the tibial defect supported bone growth, mainly on the periphery of the graft, but greater bone growth and less soft tissue invasion was observed in the avascular BMP-2 loaded scaffold implanted directly into the tibia without prior *in vivo* maturation. Histopathological evaluation noted considerably greater vascularity in the bone grafts that underwent *in vivo* maturation with an inserted vascular bundle compared with the avascular BMP-2 loaded graft. Our findings indicate that the use of an initial DCIA *in vivo* bioreactor maturation step is a promising approach to developing vascularized autologous bone grafts, although scaffolds with greater osteoinductivity should be further studied.

Keywords: large bone defect, sheep model, 3D printed scaffolds, prevascularization, *in vivo* bioreactor

Impact Statement

This translational pilot study aims at combining a tissue engineering scaffold strategy, *in vivo* prevascularization, and a modified transplantation technique to accelerate large segmental bone defect repair. First, we three-dimensional (3D) printed a 5 cm scaffold with a unique design to facilitate vascular bundle inclusion and osteoinductive growth factor delivery. Second, we established a new sheep deep circumflex iliac artery model as an *in vivo* bioreactor for prevascularizing the novel 3D printed osteoinductive scaffold. Subsequently, we transplanted the prevascularized bone graft to a clinically relevant 5 cm segmental bone defect in the sheep tibia for bone regeneration.

Departments of [1]Orthopaedic Surgery, [2]Material Science and Engineering, and [3]Bioengineering, Stanford University, Stanford, California, USA.
Departments of [4]Mechanical Engineering and School of Biomedical Engineering, [5]Clinical Sciences, and [6]Microbiology, Immunology, and Pathology, Colorado State University, Fort Collins, Colorado, USA.
Departments of [7]Chemistry and [8]Mechanical Engineering, Stanford University, Stanford, California, USA.

Introduction

Repair of large bone defects remains a significant clinical challenge. Each year, more than half a million people in the United States require bone grafting to achieve healing.[1–3] Bone defects that cannot heal on their own, even when given appropriate fixation, are termed ''critical sized defects.'' These large defects, typically considered >4–5 cm, are very difficult to treat and require complicated reconstructive procedures. Successful repair of large defects has been achieved by techniques such as distraction osteogenesis,[4,5] induced membrane,[6,7] and vascularized fibula grafting,[8,9] but patients still frequently suffer from substantial long-term disability, discomfort, and even amputation due to treatment failure. Among the clinically available treatments, vascularized autogenous bone grafts such as free fibular grafts allow the cells contained within the grafted tissue (e.g., mesenchymal stem cells, osteoblasts, and osteoclasts) to remain viable, by virtue of maintaining their blood supply via surgical anastomosis between the blood vessels of the graft tissue and recipient site.[10]

In retrospective studies of critical-sized defects, rates of union after vascularized free fibular grafting range from 70% to 100%.[11–18] The mean time to union is ~6 months.[11,14,15,17] The rate of return to weight-bearing and adequate functionality, when reported, is also generally high: one study reporting it to be 96%.[19] However, the rate of fractures after free fibular grafting in the lower extremities range from 15% to more than 40%[8,11,13,14] because the donor grafts do not match the anatomical geometry or mechanical properties of the recipient site. As with all autografts, vascularized fibular grafts are also associated with donor site morbidity.

The inherent limitations of autogenous grafting and standard reconstructive procedures have led to the emergence of tissue engineering, in which scaffolds, growth factors, and stem cells are used alone or in combination to repair tissues and restore function.[20,21] Customized tissue-engineered bone grafts could remove the risks of donor site morbidity and the mismatch of anatomical shape and mechanical properties observed with fibular grafts. Such customized implants can be readily prepared by three-dimensional (3D) printing technologies, using well-described techniques involving synthetic scaffolds made from composites of calcium phosphate and organic polymers.

We recently conducted a series of studies to systematically determine the impact of individual fabrication parameters on the final properties of 3D printed scaffolds composed of polycaprolactone (PCL) and β-tricalcium phosphate (β-TCP).[22,23] We have successfully employed our 3D printed composite scaffolds to reconstruct critical-sized segmental bone defects in rats[24] and large channels in the rabbit femoral head under both healthy and osteonecrotic conditions.[25,26]

Achieving timely and effective vascularization arguably remains the greatest challenge, preventing the translation of most tissue engineered constructs to clinical practice.[27–30] Prevascularization of anatomically shaped, large synthetic grafts either *in vitro* or *in vivo* has been explored as a strategy to accelerate the establishment of blood flow and functional graft integration with host tissue on implantation.[31–33] *In vivo* prevascularization takes advantage of the *de novo* vascularization process, which occurs in synthetic grafts during a preliminary period of implantation, to generate autologously vascularized engineered tissue grafts.[31–38]

Briefly, an anatomically shaped synthetic graft is first implanted in a vasculature-enriched ectopic site such as a muscle pouch in a remote location of the body, where the synthetic graft encourages both ossification and blood vessel invasion from surrounding vascular beds. After the vascularized ossified tissue matures, the prevascularized graft can then be harvested and transferred to the defect site. The major advantage of this technique is that it harnesses endogenous vascular regenerative processes to circumvent the considerable challenge of fabricating functional vasculature within an artificial construct. *In vivo* prevascularization has previously been successfully used to prepare custom bone grafts for the repair of large mandibular discontinuity defects in animal models and human patients.[31–33,39–43]

The current study aims at combining a novel tissue engineering scaffold strategy, *in vivo* prevascularization, and a modified transplantation technique to accelerate large segmental bone defect repair and restoration of weight-bearing function. The objectives of this parametric feasibility study were three fold: First, we developed a 3D printed scaffold with a unique design to facilitate vascular bundle inclusion and osteoinductive growth factor delivery. Second, we established a novel sheep deep circumflex iliac artery (DCIA) model as an *in vivo* bioreactor for prevascularizing the novel 3D printed osteoinductive scaffold to a vascularized bone graft. The effects of implantation durations between 8 and 12 weeks on vascular bed development and ectopic bone formation during this stage were examined. Subsequently, we transplanted the prevascularized bone graft after an 8 week implantation in the DCIA muscle pouch to a 5 cm segmental bone defect in the sheep tibia for six months and used an avascular 3D printed osteoinductive scaffold as a control. The two-phase operation is shown in Figure 1.

Materials and Methods

Scaffold design

A tibia bone was extracted from an adult sheep cadaver. It was imaged by micro-computed tomography (micro-CT; eXplore CT120; TriFoil Imaging, Chatsworth, CA) to obtain its 3D geometry. Using OsiriX Lite (Pixmea SARL, Geneva, Switzerland), cross-sectional images along 12 centimeters of the diaphysis of the femur were computed. The average outer diameter was then obtained by using simple image processing with MATLAB R2016b (The MathWorks, Inc., MA), which was used as a reference for the outer diameter of a 3D printed scaffold designed in Solidworks (Dassault Systèmes, Vélizy-Villacoublay, France). The 3D printed scaffold consists of a porous tube, built up using an alternating layer-by-layer crisscross pattern. The diameter of the central channel was sized to accommodate a metal intramedullary rod for graft fixation. A row of flexible hooks aligned end-to-end longitudinally on the outer surface of the scaffold formed a semi-enclosed side channel, as shown in Figure 2B.

Material synthesis

The PCL/β-TCP composite is synthesized as follows. PCL (M_n 80,000 g/mol; Sigma-Aldrich, St. Louis, MO) and β-TCP (granule size 100 nm; Berkeley Advanced Materials, Inc., Berkeley, CA) were separately mixed in dimethylformamide solvent at 70°C for 3 h. Both solutions

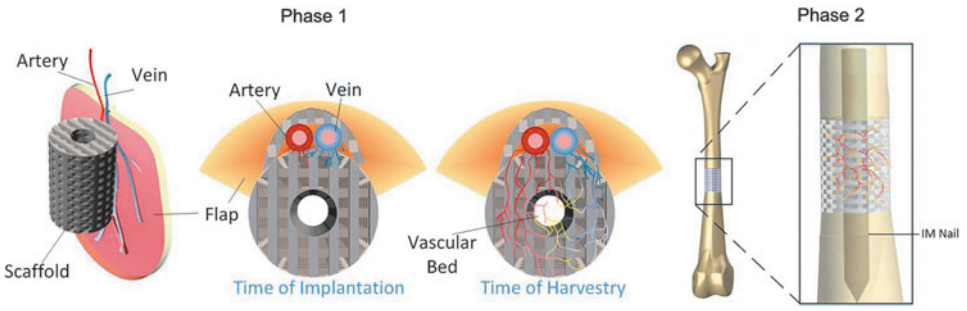

FIG. 1. Schematic of engineered vascularized bone graft development in an *in vivo* bioreactor and subsequent transplantation to tibial defect. In Phase 1, the osteoinductive growth factor-impregnated 3D printed scaffold was implanted into the vascular enriched muscle pouch to allow for microvascular invasion, whereas the osteoinductive factor in the scaffold promoted ectopic bone formation. In Phase 2, after maturation, the vascularized bone graft was transplanted into a critical segmental tibial defect to accelerate bone healing and restoration of function. 3D, three-dimensional.

were then mixed together to obtain a ratio of 80% PCL to 20% β-TCP. This combined mixture was agitated for 1 h at 70°C before being precipitated in water to remove the solvent. The material was dried for 24 h in a ventilated environment before being processed into pellets. These pellets were then melted and extruded to form a filament for fused deposition modeling (FDM) 3D printing.

3D printing of scaffolds

PCL/β-TCP scaffolds ~5 cm long and 2.0 cm in diameter were printed by FDM in a layer-by-layer fashion by using Lulzbot Mini (Aleph Objects, Inc., Loveland, CO) with a nozzle at 500 μm in diameter. Each layer is composed of parallel struts 350–400 μm in width and 200 μm tall (the height of the layer). The distance between struts was set to 1.2 mm, defining a porosity of 65% for the scaffold. Struts of consecutive layers are oriented 90° with respect to each other, to form a highly porous scaffold with interconnected pores. Once manufactured, the scaffolds were surface treated by immersing them for 12 h in a sodium hydroxide solution (5 M) at room temperature. This surface etching process results in improving hydrophilicity, as well as creating nano-pores on the surface of the struts for better cell

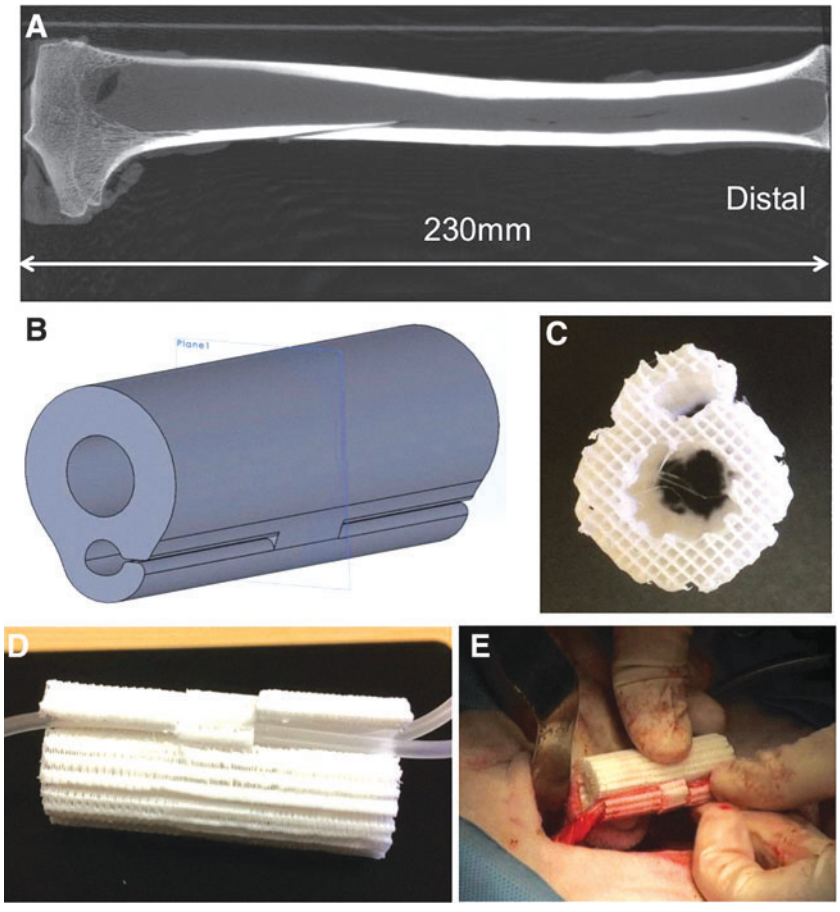

FIG. 2. Sheep tibia and 3D printed polycaprolactone/β-tricalcium phosphate scaffold with side-hooks. **(A)** A representative micro-computed tomography image of a sheep tibia; **(B)** computer model of the scaffold geometry; **(C)** *top* view of the scaffold after manufacturing; **(D)** a scaffold contains two plastic tubes to illustrate vascular bundle placement; and **(E)** the scaffold with deep circumflex iliac artery and accompanying vein during implantation.

attachment.[44,45] The 3D printed scaffold macropore size, strut thickness, and overall porosity were assessed by scanning electron microscopy and micro-CT analysis.

In vivo

Seven female Columbia-Rambouillet sheep were used in this study. Study approval was granted by the Colorado State University Institutional Animal Care and Use Committee (IACUC #17-7092A). Four animals were used for Phase 1 study, and three animals were used for Phase 2 study (Fig. 1). For the Phase 1 study, four sheep were implanted with scaffolds around the left and right DCIAs. Briefly, each animal was placed under general anesthesia and positioned in left lateral recumbency. A 10 cm dorsoventral incision was made from 1 cm below the tube coxae toward the stifle, along the tensor fascia lata. The incision was extended through the skin, subcutaneous fat, anniculus, and deep fat until the anterior border of the tensor fascia lata was visualized. The main trunk of the DCIA and accompanying vein were located and retracted. One scaffold was then placed within the iliac region around the DCIA. Routine closure of the iliac region was performed, and the animal was repositioned in right lateral recumbency. The procedure was then repeated with a second scaffold on the right side of the animal. Within each animal, one scaffold was left as described whereas the second scaffold was combined with a collagen sponge dosed with 5.4 mg recombinant human bone morphogenic protein 2 (BMP-2; Medtronic, Minneapolis, MN), inserted into the graft's central channel. After surgery, animals were allowed to eat and move *ad libitum* and were sacrificed after 8 or 12 weeks (two animals each). These durations were selected to investigate ectopic bone formation at timepoints considered typical for prevascularized bone graft formation in large animals.[31,40,46–48]

For the Phase 2 study, two additional animals were implanted with identical scaffolds treated with BMP-2 whereas the same procedure was followed to implant the scaffold around the left and right DCIAs. Scaffolds were harvested after an 8 week healing period. The left scaffold from each animal was analyzed for bone formation, and the right scaffold was implanted in a 5 cm long mid-diaphyseal tibial bone resection in the same animal created at the time of scaffold transfer. The tibial fracture was stabilized with an 8 mm diameter × 197 cm long tibial nail (I-Loc; BioMedtrix, LLC, Whipany, NJ) inserted in normograde fashion from the proximal tibia and inserted one third of the length down the tibial diaphysis.

Based on the results of the Phase 1 study, the sacrifice timepoint was extended to 24 weeks for both animals to allow for additional bone healing. One animal was sacrificed early at 13 weeks due to critical bending of the intramedullary nail, and the second animal was sacrificed 24 weeks after the tibial defect surgery. A final animal was included that underwent the same tibial defect surgery and repair with a BMP-2 treated scaffold; however, the scaffold did not undergo the initial 8 week iliac DCIA procedure. The animal was sacrificed 24 weeks after surgery.

Ex vivo

Micro-CT. Micro-CT scanning was performed on whole, dissected 5 cm long scaffolds at a resolution of 37 μm (Scanco micro-CT 80; Scanco USA, Inc., Wayne, PA). Harvested scaffolds were stored and scanned in 10% neutral buffered formalin (NBF). Bone content of each scaffold was quantitatively analyzed within the scaffold struts, the intramedullary canal, and around the scaffold periphery (Supplementary Fig. S1). The bone volume (BV) fraction (BV/TV) was calculated as the volume of bone (BV) in the scaffold region of interest (ROI) normalized to the total volume (TV) of the scaffold ROI and reported as a percentage (%). Scaffold volume was calculated as the volume of scaffold (SV) in the scaffold ROI normalized to the TV of the scaffold ROI (SV/TV).

In addition, the percentage of new bone formed during the study period in scaffolds implanted in the tibia was calculated by summing the BV formed in the scaffold and surrounding peripheral callus volume and normalizing to the volume of bone originally contained in the tibia before the creation of the ostectomy defect. This original tibial volume was determined by scanning a healthy tibia and calculating the BV within the middle 5 cm of the bone that was replaced by scaffold in the treated limbs.

Histology, histomorphometry, and histopathology. After complete fixation in 10% NBF, all samples were processed by using standard techniques for undercalcified histological analysis. Tissue was embedded in Acrylosin hard resin (Dorn and Hart Microedge, Inc., Loxley, AL). Initial cuts were taken in the sagittal plane by using a diamond blade band saw, ground to a final thickness of ~70 μm, and polished. Slide sections encompassed the entire scaffold and surrounding bone. Three slides were produced from each sample. Slides were first stained with Sanderson's Rapid Bone stain, which provided differentiation of cells within the section and allowed detection of cartilage within the tissue. Slides were then counterstained by using a Van Gieson bone stain that allowed differentiation of collagen and detection of bone (immature woven bone and mature lamellar bone) within the section.

Calibrated digital images were captured at 10× magnification and analyzed for each slide by using ImagePro Premier software (Media Cybernetics, Silver Spring, MD). The percent area of bone, soft tissue, and scaffold was calculated within the scaffold, and the absolute area of bone was calculated in the peripheral area of the scaffold (Supplementary Fig. S2). The values computed for each of the three slide sections were averaged for each scaffold.

Stained histology sections of the scaffolds implanted in the Phase 2 tibial defect animals were semi-quantitatively evaluated by a board-certified veterinary pathologist for treatment safety and efficacy, including bone formation and inflammation. The pathologist was blinded to the treatment group. The sections were analyzed and graded on a 0–4 scale according to infiltrating cell type density, where 0 indicated no cellular presence and 4 indicated the greatest amount of cellular density. The cellular parameters assessed included osteoblast cells, osteoclast cells, polymorphonuclear cells, lymphocytes, plasma cells, macrophages, giant cells, neovascularization, and implant degradation as shown in Table 1. The cumulative inflammation score was calculated as the sum of the scores of the polymorphonuclear cell, lymphocyte, plasma cell, macrophages, and giant cell categories. In addition, bone (mineralized tissue, not fibrous connective tissue) filling of each scaffold ROI (not including the scaffold periphery) was assessed on a 0–4 scale, where

Table 1. Histology Sections Analyzed and Graded Using the ISO 10993-6 Annex E Criteria for the Biological Evaluation of the Local Effects of Medical Devices on a 0–4 Scale According to Cell Type and Response

	Score				
Cell type/response	*0*	*1*	*2*	*3*	*4*
PMNs	None	Rare, 1–5/HPF	5–10/HPF	Heavy infiltrate	Packed
Lymphocytes	None	Rare, 1–5/HPF	5–10/HPF	Heavy infiltrate	Packed
Plasma cells	None	Rare, 1–5/HPF	5–10/HPF	Heavy infiltrate	Packed
Macrophages (Mφ)	None	Rare, 1–5/HPF	5–10/HPF	Heavy infiltrate	Packed
Giant cells	None	Rare, 1–2/HPF	3–5/HPF	Heavy infiltrate	Sheets
Necrosis	None	Minimal	Mild	Moderate	Severe
Osteoblastic cells[a]	None	Minimal	Mild	Moderate	Severe[a]
Signs of bone remodeling by osteoclasts[b]	None	Minimal	Mild	Moderate	Severe[b]
Neovascularization[c]	None	Minimal	Mild	Moderate	Severe[c]
Fibrosis	None	Minimal	Mild	Moderate	Severe
Signs of implant degradation	None	Minimal	Mild	Moderate	Severe
Particulate debris	None	Minimal	Mild	Moderate	Severe

The cumulative inflammation score was calculated as the sum of the scores of the PMN, lymphocyte, plasma cell, macrophages, and giant cell categories.
[a]Osteoblastic cells (OB)—severe suggests numerous OB cells.
[b]Signs of bone remodeling by osteoclasts—severe suggests abundant bone remodeling present.
[c]Neovascularization—severe suggests numerous neovascular vessels.
HPF, per high powered field; PMN, polymorphonuclear cell.

0 indicated no filling, 1 indicated <25% filling, 2 indicated 25–50% filling, 3 indicated >50% filling, and 4 indicated complete filling of the implant.

Data are presented as means ± standard deviation when sufficient sample sizes are available.

Results

Novel scaffold design and manufacturing

To accommodate a vascular bundle from the adjacent iliac region to promote microvascular invasion into the porous 3D printed constructs, we designed a unique scaffold with a semi-enclosed longitudinal channel formed by flexible hooks. As shown in Figure 2B, the geometry of the device consisted of a hollow cylinder with dimensions (outer diameter 20 mm, inner diameter 9 mm, length 50 mm) selected by considering sheep tibial anatomy and clinically available intramedullary (IM) nail sizes. The central channel of the cylinder (Fig. 2C) was used to contain a BMP-2 loaded absorbable collagen sponge (Infuse™ bone graft) to induce ectopic bone formation in the free bone flap stage, and it was then used for accommodating the IM nail in the segmental bone defect repair stage. The hinged side of the scaffold's three aligned hooks on the outer surface of the cylinder alternated to more securely hold an inserted vascular bundle consisting of the DCIA and accompanying vein, as seen in Figure 2D and E, and to provide continuous protection for the vessels during graft maturation.

Analysis by micro-CT found 73 ± 2% porosity, 729 ± 4 μm pore size, and 371 ± 13 μm strut thickness, with possible overestimation of porosity due to density averaged voxels at the interface between air and PCL/β-TCP falling below the threshold density of the bulk material. Also, measurement by a scanning electron microscope showed the consistent results of the average pore size and strut thickness of the 3D printed scaffolds to be 820 ± 23 and 380 ± 28 μm, respectively.

Micro-CT

Within the scaffold struts, BV and the BV fraction (BV/TV) were greatest for the scaffold loaded with BMP-2 that underwent tibial implantation without the inserted vascular bundle and iliac pouch bioreactor step (1562.6 mm^3 and 17.2%, respectively) followed by the scaffolds with BMP-2 that underwent 12 weeks of iliac pouch implantation only (1033.6 ± 50.2 mm^3 and 9.5 ± 1.2%, respectively) (Table 2 and Supplementary Fig. S3).

Phase 1 scaffolds that were implanted with the DCIA bundle and not dosed with BMP-2 did not demonstrate bone growth regardless of whether they were implanted for 8 or 12 weeks. The scaffold volume fraction was similar for all implants and ranged from 30.7 ± 10.7% in the scaffolds dosed with BMP-2 that were implanted in the iliac pouch for 8 weeks to 39.1 ± 12.6% in the scaffolds implanted in the iliac pouch for 8 weeks without BMP-2. The average scaffold volume fractions after muscle pouch implantation and tibia defect transplantation are 35.2 ± 8.1% and 33.0 ± 5.9%, respectively, suggesting a slow degradation rate when considering the scaffold volume fraction was ~35% with 65% porosity before implantation. However, these scaffold values after implantation by micro-CT analysis were actually greater than the non-implanted scaffold volume (27%) with 73% porosity before implantation. This discrepancy may suggest the challenges in differentiating mineral tissues and scaffolds within explants by using micro-CT analysis.

Bone growth around the periphery of the scaffolds was greatest in the scaffold dosed with BMP-2 and implanted only in the tibia (10,664.3 mm^3) followed by the scaffold dosed with BMP-2 implanted in the iliac pouch for 8 weeks and subsequently implanted in the tibia for 24 weeks (7330.9 mm^3). Minimal peripheral bone was present in the other treatment groups. The combined scaffold and peripheral BV was again greatest in the scaffold dosed with BMP-2 and implanted only in the tibia

Table 2. Micro-Computed Tomography Outcome Data

Sacrifice timepoint	*Sample treatment*	*Scaffold bone volume fraction (%)*	*Scaffold volume fraction (%)*	*Scaffold bone volume (mm^3)*	*Peripheral scaffold bone volume (mm^3)*	*Total bone volume (mm^3)*	*New bone volume fraction (%)*
Iliac: 8 weeks	Iliac DCIA implantation	0.0	48.0	0.3	0	0.3	0.0
Iliac: 8 weeks	Iliac DCIA implantation	0.0	30.2	0.3	0	0.3	0.0
	Mean ± standard deviation	**0.0 ± 0.0**	**39.1 ± 12.6**	**0.3 ± 0.0**	**0.0 ± 0.0**	**0.3 ± 0.0**	**0.0 ± 0.0**
Iliac: 8 weeks	Iliac DCIA implantation + BMP-2	2.1	23.2	0.0	0	3.2	0.0
Iliac: 8 weeks	Iliac DCIA implantation + BMP-2	4.9	38.3	502.2	603.3	1148.8	4.9
Iliac: 8 weeks	Iliac DCIA implantation + BMP-2	2.0	34.5	53.2	0	81.7	0.9
Iliac: 8 weeks	Iliac DCIA implantation + BMP-2	4.6	49.4	568.6	0	585.6	4.7
	Mean ± standard deviation	**3.4 ± 1.5**	**36.3 ± 10.8**	**281 ± 295.8**	**150.8 ± 301.7**	**454.8 ± 529.7**	**2.6 ± 2.5**
Iliac: 12 weeks	Iliac DCIA implantation	0.0	31.2	0.1	0	0.1	0.0
Iliac: 12 weeks	Iliac DCIA implantation	0.0	32.4	0.1	0	0.1	0.0
	Mean ± standard deviation	**0.0 ± 0.0**	**31.8 ± 0.8**	**0.1 ± 0.0**	**0.0 ± 0.0**	**0.1 ± 0.0**	**0.0 ± 0.0**
Iliac: 12 weeks	Iliac DCIA implantation + BMP-2	8.7	31.0	998.1	0	1117.8	8.7
Iliac: 12 weeks	Iliac DCIA implantation + BMP-2	10.4	34.1	1069.1	91.1	1267.3	11.3
	Mean ± standard deviation	**9.5 ± 1.2**	**32.5 ± 2.2**	**1033.6 ± 50.2**	**45.6 ± 64.4**	**1192.5 ± 105.7**	**10 ± 1.8**
Iliac: 8 weeks + tibia: 13 weeks	Iliac DCIA Implantation, tibia Implantation + BMP-2	**4.5**	**38.8**	**329.0**	**429.6**	**874.5**	**10.3**
Iliac: 8 weeks + tibia: 24 weeks	Iliac DCIA Implantation, tibia Implantation + BMP-2	**1.3**	**27.1**	**157.6**	**7330.9**	**7494.4**	**59.3**
Tibia: 24 weeks	Tibia implantation + BMP-2	**17.2**	**33.1**	**1562.6**	**10664.3**	**12226.9**	**134.8**

Individual scaffold data are presented. Means and standard deviations are presented in bold when treatments included more than one scaffold. The scaffold dosed with BMP-2 and implanted directly in the tibia for 24 weeks demonstrated the greatest fraction of bone in the scaffold and total bone volume of any scaffold treatment. Scaffold volume fraction, an indicator of scaffold degradation, was similar across treatments.

BMP-2, bone morphogenic protein 2; DCIA, deep circumflex iliac artery.

($12{,}226.9\,mm^3$) without prior iliac pouch maturation, which resulted in an increased final BV of 134.8% over the original tibia bone segment.

Histomorphometry

Representative hematoxylin and eosin staining of the non-decalcified 3D printed scaffold explants in Figure 3 shows newly formed mineralized tissue within the recombinant human BMP-2 (rhBMP-2) loaded scaffolds, whereas there was minimal mineralized tissue within the scaffolds in the absence of rhBMP-2 at either 8 or 12 weeks after implantation. Similar to the micro-CT findings, histomorphometric analysis found that the bone area fraction (BV/TV) within the scaffold was greatest in the scaffold dosed with BMP-2 and implanted only in the tibia (28.7%) followed by the scaffolds dosed with

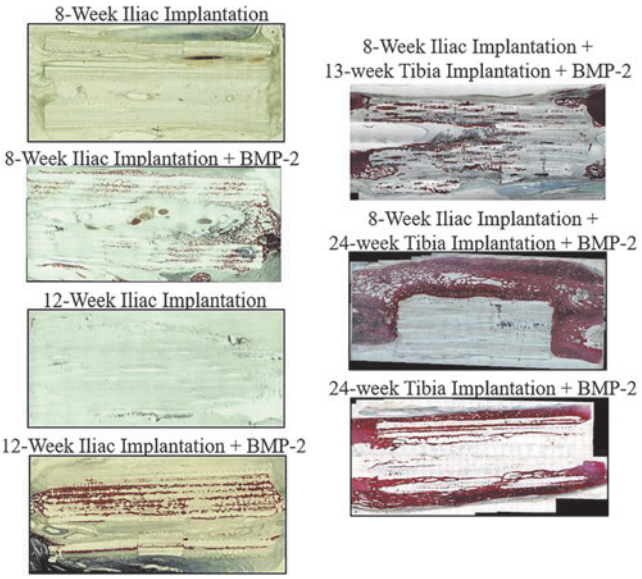

FIG. 3. Representative hematoxylin and eosin staining histology slide images from the seven scaffold treatments. *Red* indicates mineralized bone.

BMP-2 that underwent 12 weeks of iliac pouch implantation with no Phase 2 surgery (13.3 ± 5.3%) (Table 3 and Supplementary Fig. S4). Again, scaffolds not treated with BMP-2 demonstrated no bone growth in the scaffold. The lowest scaffold area fraction was in the scaffold dosed with BMP-2 and implanted only in the tibia (14.7%), and the greatest scaffold area fraction was measured in scaffolds implanted in the iliac pouch for 8 weeks with no additional treatment (28.1 ± 0.2%).

Soft tissue area fraction in the scaffold region was lowest in the scaffold dosed with BMP-2, implanted in the iliac pouch for 8 weeks, and then transferred to the tibial defect for 13 weeks (51.7%) and it was greatest in scaffolds implanted in the iliac DCIA for 12 weeks with no additional treatment (79.1 ± 12.9%).

Peripheral scaffold bone area was greatest in the scaffold dosed with BMP-2, implanted in the iliac pouch for 8 weeks, and subsequently implanted in the tibia for 24 weeks (441.2 mm^2) and the scaffold dosed with BMP-2 and implanted only in the tibia (260.9 mm^2). The ratio of peripheral bone area to bone area within the scaffold implant was greatest in these two scaffold samples as well. The peripheral bone area to scaffold bone area was 170% for the scaffold dosed with BMP-2 and implanted directly into the tibia.

The ratio of peripheral bone area to bone area within the scaffold implant was 2,228% in the scaffold dosed with BMP-2, implanted in the iliac pouch for 8 weeks, and then implanted into the tibia, a very high amount due to the limited amount of bone formed within the scaffold.

TABLE 3. HISTOLOGY OUTCOME DATA

Sacrifice timepoint	*Treatment*	*Bone area fraction (%)*	*Scaffold area fraction (%)*	*Soft tissue area fraction (%)*	*Peripheral bone area (mm^2)*	*Peripheral bone area/ implant bone area (%)*
Iliac: 8 weeks	Iliac DCIA implantation	0.0	28.2	71.6	0.0	0.0
Iliac: 8 weeks	Iliac DCIA implantation	0.0	27.9	72.1	0.0	0.0
	Mean ± standard deviation	**0.0 ± 0.0**	**28.1 ± 0.2**	**71.8 ± 0.3**	**0.0 ± 0.0**	0 ± 0
Iliac: 8 weeks	Iliac DCIA implantation + BMP-2	6.6	32.5	61.0	3.6	11.5
Iliac: 8 weeks	Iliac DCIA implantation + BMP-2	4.6	23.4	70.8	0.0	0.0
Iliac: 8 weeks	Iliac DCIA implantation + BMP-2	4.7	32.0	63.3	7.8	24.4
Iliac: 8 weeks	Iliac DCIA implantation + BMP-2	5.6	32.8	61.6	0.0	0.0
	Mean ± standard deviation	**5.4 ± 0.9**	**30.1 ± 4.5**	**64.2 ± 4.6**	**2.9 ± 3.7**	**9 ± 11.6**
Iliac: 12 weeks	Iliac DCIA implantation	0.0	30.4	69.9	0.0	0.0
Iliac: 12 weeks	Iliac DCIA implantation	0.0	11.8	88.2	0.0	0.0
	Mean ± standard deviation	**0.0 ± 0.0**	**21.1 ± 13.2**	**79.1 ± 12.9**	**0.0 ± 0.0**	**0.0**
Iliac: 12 weeks	Iliac DCIA implantation + BMP-2	9.6	22.3	68.1	0.0	0.0
Iliac: 12 weeks	Iliac DCIA implantation + BMP-2	17.1	27.1	55.8	31.6	38.6
	Mean ± standard deviation	**13.3 ± 5.3**	**24.7 ± 3.4**	**61.9 ± 8.7**	**15.8 ± 22.4**	**19.3 ± 27.3**
Iliac: 8 weeks + tibia: 13 weeks	Iliac DCIA implantation, tibia implantation + BMP-2	**8.5**	**39.7**	**51.7**	**10.1**	**18.5**
Iliac: 8 weeks + tibia: 24 weeks	Iliac DCIA implantation, tibia implantation + BMP-2	**2.6**	**35.8**	**61.6**	**441.2**	**2228.2**
Tibia: 24 weeks	Tibia implantation + BMP-2	28.7	14.7	56.7	260.9	170.0

Means and standard deviations are presented in bold when treatments included more than one scaffold. The scaffold dosed with BMP-2 and implanted directly in the tibia for 24 weeks demonstrated the greatest fraction of bone in the scaffold and peripheral bone area of any scaffold treatment. Soft tissue area within the scaffolds was similar across scaffold treatments.

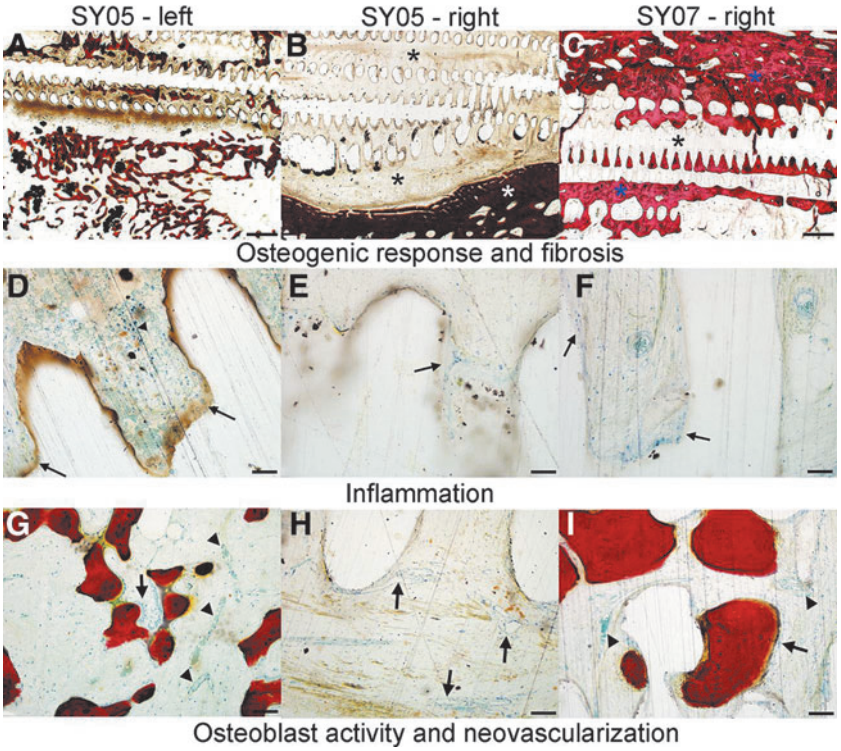

FIG. 4. Representative photomicrographs of ISO-10993-6 histological scoring parameters. **(A–C)** Osteogenic response and fibrosis scoring. **(A)** Animal SY05-left. Photomicrograph demonstrating an osteogenic response score of 2 (mild; 25–50% bone filling of implant/site) and a fibrosis score of 2 (mild), characterized by thin anastomosing trabeculae of new bone being laid down directly on a fibrous tissue intermediate that has permeated the implant. Dense fibrous connective tissue comprises the remaining implant associated new tissue. **(B)** Animal SY05-right. Photomicrograph demonstrating an osteogenic response score of 0 (none), and a fibrosis score of 3 (moderate). New host tissue growing into the implant is composed entirely of dense fibrosis (*black asterisks*), whereas the only visible bone is pre-existing tibial bone of the implant site. **(C)** Animal SY07-right. Photomicrograph demonstrating an osteogenic response score of 2 (mild; 25–50% bone filling of implant/site) and a fibrosis score of 1 (minimal). Abundant new bone composed of densely packed trabeculae (*blue asterisks*) infiltrates the implant material/void space left by the implant. The remaining space between the new bone is filled with increased amounts of adipose tissue, with only minimal fibrous tissue (*black asterisk*). **(A–C)** are 1.25×magnification, scale bar = 1 mm. **(D–F)** Inflammation. **(D)** Animal SY05-left. Photomicrograph demonstrating a cumulative inflammation score 6. Multifocally, low to moderate numbers of lymphocytes (*arrowhead*) and multi-nucleate giant cells (*arrows*) infiltrate the fibrous tissue immediately surrounding the implant-associated void space. **(E)** Animal SY05-right. Photomicrograph demonstrating a cumulative inflammation score of 3/20. Inflammation is predominately composed of a few giant cells (*arrows*) infiltrating the fibrous tissue immediately adjacent to implant void spaces. **(F)** Animal SY07-right. Photomicrograph demonstrating a cumulative inflammation score of 2/20. Similar to SY05-right, inflammation in this animal was characterized primarily by few scattered giant cells (*arrows*) present throughout the fibrous tissue surrounding the implant/void space. Images **(D–F)** are 20×magnification, scale bar = 50 μm. **(G–I)** Osteoblast activity and neovascularization. **(G)** Animal SY05-left. Photomicrograph demonstrating an osteoblast activity score of 2 and a neovascularization score of 1. A single layer of plump reactive osteoblasts (*arrow*) segmentally line endosteal surfaces of new bone. There is a minimal degree (~1–2 vessels per 20×magnification field) of new blood vessel formation (*arrowheads*). **(H)** Animal SY05-right. Photomicrograph demonstrating an osteoblast activity score of 0 and a neovascularization score of 2. No new bone and associated osteoblast activity was observed either extending from the margin of the tibial defect or being laid down directly within the implant. There is a mild degree (~3–5 vessels per 20×magnification field) of new blood vessel formation (*black arrows*) throughout the fibrous connective tissue surrounding the implant. **(I)** Animal SY07-right. Photomicrograph demonstrating an osteoblast activity score of 1 and a neovascularization score of 1. Osteoblast activity (*arrow*) was rarely observed along endosteal surfaces of new bone. Images **(G–I)** are 10×magnification, scale bar = 100 μm.

Histopathology

Representative images demonstrating osteogenic response, fibrosis, inflammation, osteoblast activity, and neovascularization are presented in Figure 4. Cumulative inflammation was similar in scaffolds dosed with BMP-2 that underwent DCIA bundle insertion within the iliac pouch for Phase 1 only (4.2 ± 1.2) and the scaffold dosed with BMP-2 that underwent 8-week iliac pouch implantation followed by Phase 2 tibial implantation for 13 weeks (4.3) (Table 4 and Supplementary Fig. S5). Cumulative inflammation scores were lowest in the scaffold dosed with BMP-2 that underwent 8-week iliac pouch implantation followed by 24 weeks of tibial implantation (3.3) and the scaffold dosed with BMP-2 and implanted only in the tibia (2.0).

Table 4. Histopathology Outcome Data for Scaffolds Implanted in Tibia Defect Animals

Sacrifice timepoint	*Treatment*	*Cumulative inflammation score*	*Necrosis*	*Osteoblast cells*	*Osteoclast remodeling*	*Neovascularization*	*Implant degradation*	*Osteogenic response*
Iliac: 8 weeks	Iliac DCIA implantation + BMP-2	5.0	0.0	1.7	0.7	2.0	0.0	2.0
Iliac: 8 weeks	Iliac DCIA implantation + BMP-2	3.3	0.0	1.0	0.0	2.0	0.0	2.0
	Mean ± standard deviation	**4.2 ± 1.2**	**0.0 ± 0.0**	**1.3 ± 0.5**	**0.3 ± 0.5**	**2.0 ± 0.0**	**0.0 ± 0.0**	**2.0 ± 0.0**
Iliac: 8 weeks + tibia: 13 weeks	Iliac DCIA implantation, tibia implantation + BMP-2	**4.3**	**0.0**	**1.0**	**0.7**	**2.3**	**0.0**	**1.0**
Iliac: 8 weeks + tibia: 24 weeks	Iliac DCIA implantation, tibia implantation + BMP-2	**3.3**	**0.0**	**0.0**	**0.0**	**2.0**	**0.0**	**0.3**
Tibia: 24 weeks	Tibia implantation + BMP-2	**2.0**	**0.0**	**1.3**	**1.3**	**1.0**	**0.0**	**2.0**

Cumulative inflammation (the sum of scores assigned to PMN, lymphocyte, plasma cell, macrophages, and giant cell categories; maximum possible score = 20) was lowest in the scaffold dosed with BMP-2 and implanted directly in the tibia for 24 weeks. The osteogenic response was generally lower in scaffolds that underwent iliac DCIA implantation before tibia implantation. Despite increased bone formation around the scaffold periphery, the scaffold implanted directly into the tibia for 24 weeks demonstrated similar osteogenic growth in the scaffold ROI as scaffolds that were not implanted into the tibia. No signs of necrosis or implant degradation were observed within any scaffold.

ROI, region of interest.

Osteogenic response within the scaffolds (not including the peripheral scaffold area) was similar for all scaffolds (range 1.0–2.0), with the exception of the scaffold with BMP-2 that underwent 8-week iliac pouch implantation followed by 24 weeks of tibial implantation (0.3). Similarly, osteoblast cell activity was comparable for all scaffold treatments (range 1.0–1.3), again with the exception of the scaffold that underwent 8-week iliac pouch implantation followed by 24 weeks of tibial implantation (0.0). Osteoclast remodeling was greatest in the scaffold dosed with BMP-2 and implanted directly in the tibia for 24 weeks (1.3) and was similar between all other scaffolds (range 0.0–0.7). Neovascularization was lowest in the scaffold dosed with BMP-2 and implanted directly in the tibia for 24 weeks (1.0) and was similar between all other scaffolds (range 2.0–2.3). No signs of implant degradation or necrosis were observed for any scaffold.

Discussion

In this study, we developed a unique scaffold that can accommodate a vascular bundle for use in an *in vivo* bioreactor approach to engineer a vascularized bone graft, followed by transplantation into a large bone defect. As proof of concept, our study has shown first that the vascular enriched iliac region can be used as a muscle pouch implantation site (*in vivo* bioreactor) for prevascularizing a large synthetic bone graft, and second, that a clinically relevant 5 cm scaffold loaded with BMP-2 implanted into the muscular pouch can clearly form ectopic bone at 8 and 12 weeks after implantation. Third, the prevascularized bone graft after 8 weeks of maturation in the muscle pouch can be harvested and re-implanted to repair a 5 cm tibial segmental bone defect in sheep.

The engineered bone graft reconstructive procedure established in this study took place in two phases. Phase 1 implanted a composite scaffold with an inset vascular bundle within the iliac pouch to form a vascularized bone graft by inducing ectopic bone formation. In four animals, one scaffold was placed within each iliacus muscle bilaterally ($N = 2$ total scaffolds per animal). One scaffold per animal was left untreated, whereas the second scaffold was loaded with BMP-2 (5.4 mg/scaffold). Two animals were sacrificed at 8 weeks and two animals were sacrificed at 12 weeks after the surgical procedure.

Micro-CT and histomorphometric analysis of the harvested grafts clearly demonstrated that minimal to no bone development occurred in scaffolds without BMP-2 treatment. With BMP-2 delivery, significant levels of vascularized bone tissue were observed, with greater bone tissue development in the scaffolds implanted for 12 weeks compared with those only implanted for 8 weeks. It has been reported that due to lacking mechanical loading, the ectopic bone formation may experience bone resorption over time.[46] These findings suggest further study to identify the potentially optimal duration for autologous bone graft prevascularization in the iliac pouch to balance new ectopic bone formation induced by BMP-2 and resorption due to lack of mechanical stimulation in an ectopic area.

In Phase 2, sheep tibial defect reconstruction was performed to evaluate whether the harvested prevascularized bone grafts could be transplanted to repair a large bone defect. Three animals were utilized to investigate Phase 2 healing in a 5 cm tibial defect. Two of the animals first underwent the same Phase 1 iliac muscle implantation procedure with BMP-2 loaded scaffolds for 8 weeks as previously described, followed by a second procedure in which one scaffold was removed from the iliac pouch and re-implanted in a 5 cm diaphyseal defect in the tibia. Of these two prevascularized bone grafts, one was implanted for 13 weeks and one for 24 weeks before harvest and analysis of bone healing. A third animal underwent the same tibial defect procedure without the Phase 1 flap maturation step, receiving an avascular 3D printed composite scaffold with BMP-2, which was harvested at 24 weeks after implantation.

Micro-CT evaluation of bone regeneration in the tibial defect demonstrated that despite maturation in the iliac pouch, the prevascularized bone grafts failed to induce as much internal, peripheral, or total bone growth when implanted in the tibia as the avascular scaffold. Further, histopathological review indicated that the avascular scaffold implanted directly in the tibia was the only specimen to demonstrate mature lamellar cortical bone with typical osteon structures. These results suggest the unsurprising conclusion that the iliac pouch environment is less conducive to bone development than the tibial defect, and that the BMP-2 dose, which was likely mostly or entirely depleted by the end of the prevascularization phase, was delivered to lesser effect within the muscle pouch. In addition, soft tissues that invaded the scaffold during prevascularization in the iliac pouch likely hindered later bone ingrowth in the tibial defect.

It is worth further investigation to determine whether and to what extent the invading soft tissues within scaffolds may convert to mineralized tissues in later phases. Efforts to engineer autologous bone flaps *in vivo* should either seek out regions in the body better suited to bone formation such as a periosteal pouch, or they must otherwise display improved osteoinductive potential beyond the BMP-2 delivery of the current study to better guide bone development within the muscle pouch environment.

Although less bone tissue was generated in the tibial defect by scaffolds that underwent a period of maturation in the iliac pouch compared with that induced by the avascular scaffold, application of the *in vivo* bioreactor strategy with an inserted vascular bundle dramatically increased vascularization within the newly formed bone, as seen in the histopathology scores. These are promising findings, given that the vascularization of large engineered bone grafts remains their biggest impediment to translation. In clinical scenarios, large bone defect cases are typically accompanied by trauma to the surrounding soft tissues and compromised local revascularization potential. Although osteogenesis within the constructs was not complete, our development of unique scaffolds that enable the formation of vascularized bone grafts and free bone flaps with an incorporated expendable vascular bundle represents an exciting advancement.

This investigation showed that a 5 cm clinically relevant large synthetic scaffold with BMP-2 can aid in generating bone growth when used in large defect scenarios. Although extensive vasculature and bone growth occurred in the tibia implant that first underwent iliac pouch maturation, greater bone formation occurred within the scaffold when iliac pouch implantation was not performed. Future studies to optimize scaffold design and growth factor selection, loading, dosage, and controlled release of growth factor will likely yield improved bone healing.

This study did not include any biomechanical characterization due to the limited amount of bone growth in Phase I samples and the hypothesized inability to detect meaningful mechanical differences due to soft tissue deposition within the rigid scaffolds; however, future studies investigating these parameters should also include analysis of the biomechanical characteristics of these scaffolds after implantation and healing. In addition, it is important to note that the purpose of this study was to parametrically investigate the effectiveness of this newly developed DCIA implantation technique on bone growth with numerous healing variables, including the use of BMP-2 and relocation of the DCIA scaffold to a long bone defect. Due to the nature of the study, sample sizes for this investigation were limited. Our future studies intend to investigate the most promising combinations of scaffold characteristics (DCIA implantation with long bone implantation and BMP-2) more rigorously in a statistically powered study with fewer treatment groups and greater sample sizes.

Compared with the two-phase surgical treatment, a single surgery for large bone defect repair by inserting an adjacent vascular bundle into a scaffold with an open groove or channel has been reported to promote angiogenesis and bone formation by avoiding necrosis of the center of bone scaffold or defect.[34,36,49–51] To the best of our knowledge, *in vivo* prevascularization and graft maturation in an ectopic muscle pouch to develop a vascularized bone graft or bone flap with transplantation into a critical sized bone defect as large as 5 cm has not been previously attempted. We envision that the successful *in vivo* maturation of engineered bone grafts could overcome the significant challenges with currently existing techniques in large bone defect treatment, and make breakthroughs in bone tissue engineering.

Conclusion

In summary, we have developed a unique 3D printed bone scaffold design with flexible hooks that enable rapid and surgically uncomplicated inclusion of an intact vascular bundle within the engineered construct. When implanted around the DCIA in the sheep iliac pouch for 8 or 12 weeks, scaffolds loaded with BMP-2 induced formation of vascularized mineralized bone tissue, with somewhat higher BVs observed after 12 weeks. These findings demonstrate that our DCIA model can serve as an *in vivo* bioreactor for regenerating vascularized autologous bone grafts.

The scaffolds matured in the iliac pouch were used to reconstruct a critical-sized segmental tibial defect in sheep, yielding increased vascularity but decreased total bone content compared with an avascular BMP-2 loaded scaffold implanted directly into the tibial defect, which indicates that future strategies should look into improving osteogenesis within the scaffolds during the *in vivo* bioreactor maturation stage. Nevertheless, our findings highlight the potential of 3D printed synthetic constructs to yield a highly vascularized

autologous free bone flap analogous to the vascularized fibular graft, with sufficient volume to reconstruct critical-sized bone defects but without the need to sacrifice one of the patient's skeletal bones.

Acknowledgments

Special thanks are due to Lucas Nakamura and Cecily Broomfield from the Colorado State University Orthopaedic Bioengineering Research Laboratory for histological sample preparation.

Disclosure Statement

No competing financial interests exist.

Funding Information

This research was partially funded through a generous donation from Kent Thiry and Denise O'Leary, and the financial support of National Institutes of Health grants R01AR057837, U01AR069395, R01AR072613, and R01AR074458 from National Institute of Arthritis and Musculoskeletal and Skin Diseases, and Department of Defense grant W81XWH-20-1-0343.

Supplementary Material

Supplementary Figure S1
Supplementary Figure S2
Supplementary Figure S3
Supplementary Figure S4
Supplementary Figure S5

References

1. Holzer, G., Einhorn, T.A., and Majeska, R.J. Estrogen regulation of growth and alkaline phosphatase expression by cultured human bone marrow stromal cells. J Orthop Res **20,** 281, 2002.
2. Larsson, S., and Bauer, T.W. Use of injectable calcium phosphate cement for fracture fixation: a review. Clin Orthop Relat Res **395,** 23, 2002.
3. Conway, J.D. Autograft and nonunions: morbidity with intramedullary bone graft versus iliac crest bone graft. Orthop Clin North Am **41,** 75, 2010; table of contents.
4. Hernandez-Fernandez, A., Vélez, R., Soldado, F., Saenz-Ríos, J.C., Barber, I., and Aguirre-Canyadell, M. Effect of administration of platelet-rich plasma in early phases of distraction osteogenesis: an experimental study in an ovine femur model. Injury **44,** 901, 2013.
5. Yang, J.-H., Kim, H.-J., Kim, S.-E., *et al.* The effect of bone morphogenic protein-2-coated tri-calcium phosphate/hydroxyapatite on new bone formation in a rat model of femoral distraction osteogenesis. Cytotherapy **14,** 315, 2012.
6. Masquelet, A., Fitoussi, F., Begue, T., and Muller, G. [Reconstruction of the long bones by the induced membrane and spongy autograft]. Ann Chir Plast Esthet **45,** 346, 2000 (Article in French).
7. Pelissier, P.H., Masquelet, A.C., Bareille, R., Pelissier, S.M., and Amedee, J. Induced membranes secrete growth factors including vascular and osteoinductive factors and could stimulate bone regeneration. J Orthop Res **22,** 73, 2004.
8. de Boer, H.H., and Wood, M.B. Bone changes in the vascularised fibular graft. J Bone Joint Surg **71-B,** 374, 1989.
9. Khira, Y., and Badawy, H. Pedicled vascularized fibular graft with Ilizarov external fixator for reconstructing a large bone defect of the tibia after tumor resection. J Orthop Traumatol **14,** 91,2013.
10. Beris, A.E., Lykissas, M.G., Korompilias, A.V., *et al.* Vascularized fibula transfer for lower limb reconstruction. Microsurgery **31,** 205, 2011.
11. de Boer, H.H., Wood, M.B., and Hermans, J. Reconstruction of large skeletal defects by vascularized fibula transfer. Factors that influenced the outcome of union in 62 cases. Int Orthop **14,** 121, 1990.
12. Eward, W.C., Kontogeorgakos, V., Levin, L.S., and Brigman, B.E. Free vascularized fibular graft reconstruction of large skeletal defects after tumor resection. Clin Orthop Relat Res **468,** 590, 2010.
13. Lee, K.S., Han, S.B., and Baek, J.R. Free vascularized osteocutaneous fibular graft to the tibia in 51 consecutive cases. J Reconstr Microsurg **20,** 277, 2004.
14. Minami, A., Kasashima, T., Iwasaki, N., Kato, H., and Kaneda, K. Vascularised fibular grafts. An experience of 102 patients. J Bone Joint Surg Br **82,** 1022, 2000.
15. Ozaksar, K., Sugun, T.S., Toros, T., Gurbuz, Y., Kayalar, M., and Ozerkan, F. Free vascularized fibular grafts in Type 3 open tibia fractures. Acta Orthop Traumatol Turc **46,** 430, 2012.
16. Wood, M.B., and Bishop, A.T. Massive bone defects of the upper limb: reconstruction by vascularized bone transfer. Hand Clin **23,** 49, 2007.
17. Yajima, H., Tamai, S., Mizumoto, S., and Ono, H. Vascularised fibular grafts for reconstruction of the femur. J Bone Joint Surg Br **75,** 123, 1993.
18. Zhen, P., Hu, Y.Y., Luo, Z.J., Liu, X.Y., Lu, H., and Li, X.S. One-stage treatment and reconstruction of Gustilo Type III open tibial shaft fractures with a vascularized fibular osteoseptocutaneous flap graft. J Orthop Trauma **24,** 745, 2010.
19. Aponte-Tinao, L., Farfalli, G.L., Ritacco, L.E., Ayerza, M.A., and Muscolo, D.L. Intercalary femur allografts are an acceptable alternative after tumor resection. Clin Orthop Relat Res **470,** 728, 2012.
20. Langer, R. Tissue engineering: perspectives, challenges, and future directions. Tissue Eng **13,** 1, 2007.
21. Kanczler, J., and Oreffo, R. Osteogenesis and angiogenesis: the potential for engineering bone. Eur Cells Mater **15,** 100, 2008.
22. Bruyas, A., Lou, F., Stahl, A.M., *et al.* Systematic characterization of 3D-printed PCL/β-TCP scaffolds for biomedical devices and bone tissue engineering: influence of composition and porosity. J Mater Res **33,** 1948, 2018.
23. Bruyas, A., Moeinzadeh, S., Kim, S., Lowenberg, D.W., and Yang, Y.P. Effect of electron beam sterilization on three-dimensional-printed polycaprolactone/beta-tricalcium phosphate scaffolds for bone tissue engineering. Tissue Eng Part A **25,** 248, 2019.
24. DeBaun, M.R., Stahl, A.M., Daoud, A.I., *et al.* Preclinical induced membrane model to evaluate synthetic implants for healing critical bone defects without autograft. J Orthop Res **37,** 60, 2019.
25. Maruyama, M., Nabeshima, A., Pan, C.-C., *et al.* The effects of a functionally-graded scaffold and bone marrow-derived mononuclear cells on steroid-induced femoral head osteonecrosis. Biomaterials **187,** 39, 2018.

26. Kawai, T., Shanjani, Y., Fazeli, S., *et al.* Customized, degradable, functionally graded scaffold for potential treatment of early stage osteonecrosis of the femoral head. J Orthop Res **36,** 1002, 2018.
27. Laschke, M.W., Harder, Y., Amon, M., *et al.* Angiogenesis in tissue engineering: breathing life into constructed tissue substitutes. Tissue Eng **12,** 2093, 2006.
28. Nguyen, L.H., Annabi, N., Nikkhah, M., *et al.* Vascularized bone tissue engineering: approaches for potential improvement. Tissue Eng Part B Rev **18,** 363, 2012.
29. Krishnan, L., Willett, N., and Guldberg, R. Vascularization strategies for bone regeneration. Ann Biomed Eng **42,** 432, 2014.
30. Mercado-Pagan, A.E., Stahl, A.M., Shanjani, Y., and Yang, Y. Vascularization in bone tissue engineering constructs. Ann Biomed Eng **43,** 718, 2015.
31. Terheyden, H., Jepsen, S., and Rueger, D.R. Mandibular reconstruction in miniature pigs with prefabricated vascularized bone grafts using recombinant human osteogenic protein-l: a preliminary study. Int Oral Maxillofac Surg **28,** 461, 1999.
32. Warnke, P.H., Springer, I.N.G., Wiltfang, J., *et al.* Growth and transplantation of a custom vascularised bone graft in a man. Lancet **364,** 766, 2004.
33. Tatara, A.M., Wong, M.E., and Mikos, A.G. In vivo bioreactors for mandibular reconstruction. J Dent Res **93,** 1196, 2014.
34. Vidal, L., Kampleitner, C., Krissian, S., *et al.* Regeneration of segmental defects in metatarsus of sheep with vascularized and customized 3D-printed calcium phosphate scaffolds Sci Rep **10,** 1, 2020.
35. Beier, J.P., Horch, R.E., Hess, A., *et al.* Axial vascularization of a large volume calcium phosphate ceramic bone substitute in the sheep AV loop model. J Tissue Eng Regen Med **4,** 216, 2010.
36. Vidal, L., Brennan, M.Á., Krissian, S., *et al.* In situ production of pre-vascularized synthetic bone grafts for regenerating critical-sized defects in rabbits. Acta Biomater **114,** 384, 2020.
37. Sparks, D.S., Savi, F.M., Saifzadeh, S., Schuetz, M.A., Wagels, M., and Hutmacher D.W. Convergence of scaffold-guided bone reconstruction and surgical vascularization strategies-a quest for. Front Bioeng Biotechnol **7,** 448, 2019.
38. Vidal, L., Kampleitner, C., Brennan, M., Hoornaert, A., and Layrolle, P. Reconstruction of large skeletal defects: current clinical therapeutic strategies and future directions using 3D printing. Front Bioeng Biotechnol **8,** 61, 2020.
39. Heliotis, M., Lavery, K., Ripamonti, U., Tsiridis, E., and Di Silvio, L. Transformation of a prefabricated hydroxyapatite/osteogenic protein-1 implant into a vascularised pedicled bone flap in the human chest. Int J Oral Maxillofac Surg **35,** 265, 2006.
40. Orringer, J.S., Shaw, W.W., Borud, L.J., Freymiller, E.G., Wang, S.A., and Markowitz, B.L. Total mandibular and lower lip reconstruction with a prefabricated osteocutaneous free flap. Plast Reconstr Surg **104,** 793, 1999.
41. Warnke, P.H., Wiltfang, J., Springer, I., *et al.* Man as living bioreactor: fate of an exogenously prepared customized tissue-engineered mandible. Biomaterials **27,** 3163, 2006.
42. Cheng, M.-H., Brey, E.M., Ulusal, B.G., and Wei, F.-C. Mandible augmentation for osseointegrated implants using tissue engineering strategies. Plast Reconstr Surg **118,** 1e, 2006.
43. Kokemueller, H., Spalthoff, S., Nolff, M., *et al.* Prefabrication of vascularized bioartificial bone grafts in vivo for segmental mandibular reconstruction: experimental pilot study in sheep and first clinical application. Int J Oral Maxillofac Surg **39,** 379, 2010.
44. Yeo, A., Rai, B., Sju, E., Cheong, J.J., and Teoh, S.H. The degradation profile of novel, bioresorbable PCL-TCP scaffolds: an in vitro and in vivo study. J Biomed Mater Res A **84A,** 208, 2008.
45. Yeo, A., Wong, W.J., Khoo, H.H., and Teoh, S.H. Surface modification of PCL-TCP scaffolds improve interfacial mechanical interlock and enhance early bone formation: an in vitro and in vivo characterization. J Biomed Mater Res A **92A,** 311, 2010.
46. Cheng, M.-H., Brey, E.M., Allori, A., *et al.* Ovine model for engineering bone segments. Tissue Eng **11,** 214, 2005.
47. Brey, E.M., Cheng, M.-H., Allori, A., *et al.* Comparison of guided bone formation from periosteum and muscle fascia. Plast Reconstr Surg **119,** 1216, 2007.
48. Cheng, M.-H., Brey, E.M., Allori, A.C., *et al*. Periosteum-guided prefabrication of vascularized bone of clinical shape and volume. Plast Reconst Surg **124,** 787, 2009.
49. Akita, S., Tamai, N., Myoui, A., *et al.* Capillary vessel network integration by inserting a vascular pedicle enhances bone formation in tissue-engineered bone using interconnected porous hydroxyapatite ceramics. Tissue Eng **10,** 789, 2004.
50. Wang, L., Fan, H., Zhang, Z.-Y., *et al.* Osteogenesis and angiogenesis of tissue-engineered bone constructed by prevascularized β-tricalcium phosphate scaffold and mesenchymal stem cells. Biomaterials **31,** 9452, 2010.
51. Willems, W.F., Kremer, T., Friedrich, P., and Bishop, A.T. Surgical revascularization induces angiogenesis in orthotopic bone allograft. Clin Orthop Relat Res **470,** 2496, 2012.

Address correspondence to:
Yunzhi Peter Yang, PhD
Department of Orthopedic Surgery
School of Medicine
Stanford University
240 Pasteur Drive, BMI 258
Stanford, CA 94304
USA

E-mail: ypyang@stanford.edu

Michael J. Gardner, MD
Department of Orthopedic Surgery
School of Medicine
Stanford University
240 Pasteur Drive
Stanford, CA 94304
USA

E-mail: michaelgardner@stanford.edu

Received: November 16, 2020
Accepted: March 30, 2021
Online Publication Date: June 11, 2021